Impurity Sublattice Localization in ZnO Revealed by Li Marker Diffusion

A. Yu. Azarov,[1] K. E. Knutsen,[1] P. T. Neuvonen,[1,2] L. Vines,[1] B. G. Svensson,[1] and A. Yu. Kuznetsov[1]

[1]*Department of Physics, Centre for Material Science and Nanotechnology, University of Oslo, P.O. Box 1048, Blindern, N-0316 Oslo, Norway*

[2]*Department of Physics and Astronomy-iNANO, Aarhus University, Gustav Wieds Vej 14, 8000 Aarhus C, Denmark*

(Received 25 February 2013; published 26 April 2013)

Sublattice localization of impurities in compound semiconductors, e.g., ZnO, determines their electronic and optical action. Despite that the impurity position may be envisaged based on charge considerations, the actual localization is often unknown, limiting our understanding of the incorporation and possible doping mechanisms. In this study, we demonstrate that the preferential sublattice occupation for a number of impurities in ZnO can be revealed by monitoring Li diffusion. In particular, using ion implantation, the impurity incorporation into the Zn sublattice (holds for, B, Mg, P, Ag, Cd, and Sb) manifests in the formation of Li-depleted regions behind the implanted one, while Li pileups in the region of the implantation peaks for impurities residing on O sites, e.g., N. The behavior appears to be of general validity and the phenomena are explained in terms of the apparent surplus of Zn and O interstitials, related to the lattice localization of the impurities. Furthermore, Cd + O and Mg + O co-doping experiments revealed that implanted O atoms act as an efficient blocking ''filter'' for fast diffusing Zn interstitials.

DOI: 10.1103/PhysRevLett.110.175503 PACS numbers: 61.72.uj, 61.72.Cc

The electronic configuration of an isolated atom, and its preferential lattice localization as an impurity in a crystalline solid, are obviously related. For a compound semiconductor and in a first approximation, the localization can be predicted by the electronegativity relationships. However, accounting for the availability of point defects (considering their different charge states, open volumes, etc.), the actual routes for impurity incorporation may become nontrivial. For example, there is an interpretation that Sb in ZnO may occupy Zn sites, making a complex with zinc vacancies (V_{Zn}) [1], while simplistically Sb, as a group-V element, may be anticipated to reside on oxygen sites. Thus, assuming that an impurity is introduced by ion implantation, as in many literature reports devoted to electronic doping of ZnO [2–7], dopant-defect interactions may potentially overrule the electronegativity in governing the impurity localization. However, the monitoring of actual impurity localizations, a topic having the potential to resolve electronic doping challenges in ZnO, is often neglected. The reason for this neglect is partly because of a general immaturity in understanding of doping mechanisms in ZnO, but also due to limitations of experimental techniques typically used to determine preferential lattice locations of impurities in crystalline materials. For instance, utilization of ion channeling is well established but in practice it is limited to heavy dopants at relatively high concentrations (in excess of 0.1 at. % even assuming light atomic matrixes) [8]. For some selected elements, associated nuclear reactions may be applied improving the sensitivity of channeling interpretations by a factor of 2–100, depending on the actual nuclear reaction resonance [9]. Emission channeling is another technique to study sublattice impurity locations [10], but appropriate radioactive isotopes are unavailable for many impurities of interest. On the top of these ''nuclear'' methods one could certainly consider applying extended x-ray absorption fine structure analysis [11] and electron paramagnetic resonance methods [12] having, however, their own limitations. At this end, establishing a reliable and sensitive method to discriminate between impurity sublattice occupations in ZnO is a fundamental scientific challenge that, if resolved, could have a substantial technological impact when mastering electronic doping of ZnO.

It has been shown very recently that the intrinsic point defect balance in ZnO can be dramatically shifted by implanting with either Zn or O ions [13]. The interpretation was based on striking correlations between Li redistributions and electric resistivity changes. Importantly, the appearance of surplus self-interstitials (Zn_i and O_i), in amounts corresponding to the implanted dose, resulted in two different modes for Li to redistribute: (A) forming of strongly Li depleted regions behind the implantation peaks for Zn implants or (B) accumulation of Li in the range of the implantation peak for oxygen implants. Using the methodology developed in Ref. [13], it appears logical to investigate Li redistributions in samples implanted with ions anticipated, in accordance with the electronegativity arguments, to occupy either Zn or O sublattices. If the argumentation holds, each kind of impurity might kick out the corresponding self-interstitials, so that the resulting self-interstitial surplus affects Li redistributions in either the (A) or (B) modes similar to that in self ion implanted samples [13]. Indeed, such an experiment can help to identify preferential sublattice locations for a range of impurities quoted as promising acceptors in literature.

In this work, we have undertaken individual implants for three different groups of ions: (i) typical ''Zn-like''

ions—Cd and Mg, (ii) a range of "acceptor-like" ions—N, P, Ag, and Sb, and (iii) a "donor-like" ion—B, for comparison. Moreover, in order to confirm the validity of the Li marker diffusion approach, as deduced from Ref. [13], we performed sequential Cd/Mg and O implants adjusting residual Zn_i/O_i ratios by varying the oxygen dose or its penetration depth.

10×10 mm^2, *c*-axis oriented (0001) wafers of hydrothermally grown wurtzite ZnO single crystals with a thickness of 0.5 mm, having an initial resistivity and Li concentration in the range of 0.1–0.5 kΩ cm and $2–4 \times 10^{17}$ cm^{-3}, respectively, were implanted with typical Zn- and O-substituting elements. Note, when selecting the implant parameters, there was no intention to adjust the implants to equivalent damage production, instead we explored different ion projected ranges (R_p) and dose variations irrespective of ion mass to investigate the general character of the phenomena of Li redistribution. Importantly, some of the Cd and Mg implanted samples were subjected to supplementary O implants and these samples are called "co-implants" below. The implantation parameters for the O ions were selected in order to investigate (i) the O dose dependence keeping the O and Cd ion ranges similar (Cd + O samples), or (ii) the O penetration depth dependence for the same Mg and O doses (Mg + O samples). The identification of the samples and the implantation parameters are summarized in Table I. All implants were carried out at room temperature and at 7° off the [0001] direction in order to reduce channeling. After implantation, the samples were subjected to isochronal anneals at 600–1000 °C in air [15].

Concentration versus depth profiles of the implanted impurities and Li were measured by secondary ion mass spectrometry using a Cameca IMS 7f microanalyzer. Since the present experiment resolved no redistribution of the implanted impurities at the temperatures studied, these data are not shown. For detecting Li, we used 10 keV O_2^+ ions as a primary beam rastered over the area of 150×150 μm^2. The signal-to-concentration calibration was performed using an as-implanted Li sample as reference. The conversion from the sputtering time to sample depth was performed by measuring the crater depth using a Dektak 8 stylus profilometer and assuming a constant erosion rate. In addition, the samples were analyzed by Rutherford backscattering spectrometry in channeling mode (RBS/C) with 2 MeV $^4He^+$ ions. The fraction of Cd atoms occupying substitutional positions was calculated by comparing the spectra obtained under channeling and random conditions.

Figure 1 shows (a) Li concentration versus depth profiles in Cd implanted samples before and after post-implantation annealing, while in panels (b) and (c) the Li distribution is

TABLE I. List of the implantation parameters used in the present study. Note, for co-implants (samples 8–12), we quote ^{16}O implantation parameters only, while those for ^{114}Cd and ^{24}Mg are listed in the first and second lines, respectively. The projected ranges (R_p) of implanted atoms were calculated using the TRIM code [14].

Sample #	Implants	Energy (keV)	Dose (cm^{-2})	R_p (nm)
1	^{114}Cd	300	5×10^{15}	75
2	^{24}Mg	400	6×10^{14}	500
3	^{11}B	35	1.5×10^{16}	90
4	^{15}N	50	1×10^{16}	90
5	^{31}P	900	1×10^{15}	730
6	^{107}Ag	500	5×10^{15}	120
7	^{121}Sb	1000	1×10^{15}	250
8	Cd + OLow	35	5×10^{14}	55
9	Cd + OHigh	35	5×10^{15}	55
10	Mg + O35	35	6×10^{14}	55
11	Mg + O320	320	6×10^{14}	500
12	Mg + O850	850	6×10^{14}	1000

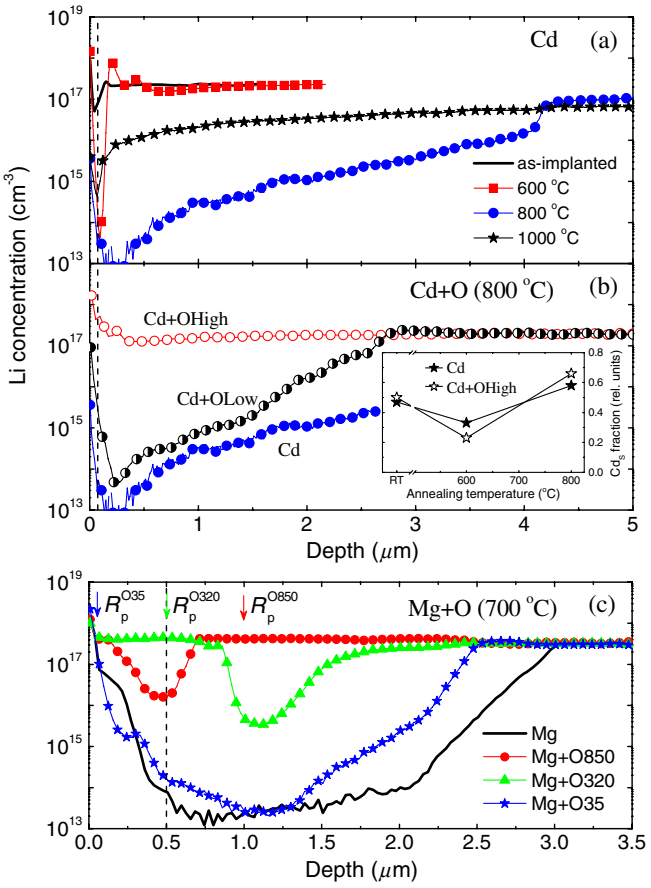

FIG. 1 (color online). Li concentration versus depth profiles in (a) Cd implanted, (b) Cd + O and (c) Mg + O co-implanted ZnO samples before and after annealing as indicated in the legends (see the Table I for the identification of the samples). Substitutional Cd fraction as a function of annealing temperature is shown in the inset in the panel (b). The projected ranges of the Cd/Mg and O ions are shown by the vertical dashed lines and arrows, respectively, in the corresponding panels.

compared for Cd/Cd + O and Mg/Mg + O implants, respectively. First, the evolution of Li profiles in Fig. 1(a) is qualitatively identical to that observed previously after Zn implantation and explained in terms of interaction of surplus Zn_i with substitutional Li (Li_{Zn}) [13]. Indeed, it is clearly seen that Li starts to move out of the implanted region already at 600 °C forming a sharp—in the scale of Fig. 1—concentration dip around R_p. Further annealing at 800 °C gives rise to a Li depleted region of at least 4 μm beyond R_p, while at higher temperature (see 1000 °C data) this region is "re-filled" by Li diffusion from the bulk. The formation of the Li depleted region is consistent with the hypothesis that implanted Cd atoms compete with Zn for substitutional sites during implantation and/or subsequent annealing, as supported by the RBS/C data in the inset in Fig. 1(b) showing substitutional (nonscattering) Cd fraction as a function of annealing temperature. As a result, a thermal dissociation of defect complexes involving Zn_i leads to the injection of surplus Zn_i which, in its turn, promote fast Li diffusion via the reaction, $Zn_i + Li_{Zn} \rightarrow Zn_{Zn} + Li_i$ upon annealing [16]. Thus, the analysis of the Cd implants alone, suggests that the appearance of the Li depletion region beyond R_p may be used as an indicator for the Cd incorporation into Zn sublattice.

In Ref. [13], the surplus of O_i in O-implanted samples was found to cause piling up of Li around R_p and, hence, it may be instructive to investigate the Li redistribution in Cd + O co-implanted samples as a function of the surplus Zn_i/O_i ratio, given by the corresponding Cd and O doses. The comparison of Cd and Cd + O co-implanted samples in Fig. 1(b) reveals that the magnitude of the Li depletion and, consequently, the amount of Zn_i surplus is strongly reduced by O co-implants, in fact, the Li redistribution is completely eliminated at a 1:1 dose ratio. This observation is extraordinary, taking into account the large mass difference between O and Cd ions and, consequently, the displacements per atom produced at a given dose. Moreover, O co-implantation is not affecting the magnitude of the substitutional Cd fraction as shown in the inset of Fig. 1(b). Therefore, the retardation (or even complete suppression) of the Li redistribution in Fig. 1(b) can be attributed to the presence of excess O itself rather than to additional disorder and/or changes in the Cd configuration caused by the O co-implants. Thus, the data in Fig. 1(b) may suggest that surplus Zn_i and O_i establish chemical bonding that suppress injection of Zn_i's (and rapid migration of Li).

Even more spectacularly, Fig. 1(c) confirms that O_i surplus behaves as a "retarding filter" for Zn_i when placed at different depths in the samples. Indeed, upon single Mg implants Li redistribution is similar to that for the Cd one, Fig. 1(a), while the depletion can be influenced by varying the position of the "oxygen filter", so that diffusing Zn_i is suppressed by O_i, similarly to that in the Cd + OHigh sample in Fig. 1(b). However, the suppression is not fully perfect and minor Li depleted regions are still detectable in Fig. 1(c) at depths where O_i does not have sufficient concentration. Further, these data support a substantially slower diffusion of O_i than of Zn_i.

Exploiting the hypothesis outlined above, we have performed additional implantations with several other elements that may potentially occupy the Zn sublattice sites, specifically Ag and B, accounting for their electron configuration in isolated states. Figs. 2(a) and 2(b) show the corresponding Li versus depth profiles upon annealing at selected temperatures (the rest of the data are omitted for clarity). As clearly seen from Fig. 2, Li is depleted from a wide region behind R_p in both samples, substantiating the hypothesis of using Li as a marker for impurity incorporation into the Zn sublattice. The mechanism governing the Li depletion in Fig. 2 is similar to that discussed above and the efficiency of different impurities X_i to occupy Zn sites might be different as reflected in corresponding formation energies of X_{Zn} [17]. However, as seen from comparison of Figs. 1(a) and 2(b) at 800 °C, the amount of Li removed from the depleted regions, normalized to the corresponding doses (ΔLi_X), for Cd ($\Delta Li_{Cd} = 0.013$) is less than half of that for B ($\Delta Li_B = 0.029$), despite an efficient Cd incorporation into the Zn sublattice, as discussed above, and a high solid solubility of Cd in ZnO [18]. Moreover, the relatively low values of ΔLi_X for both Cd and B indicate that there are other limiting factors for the Li redistribution. One such limitation may be different kinetics for the release of Zn_i's from their

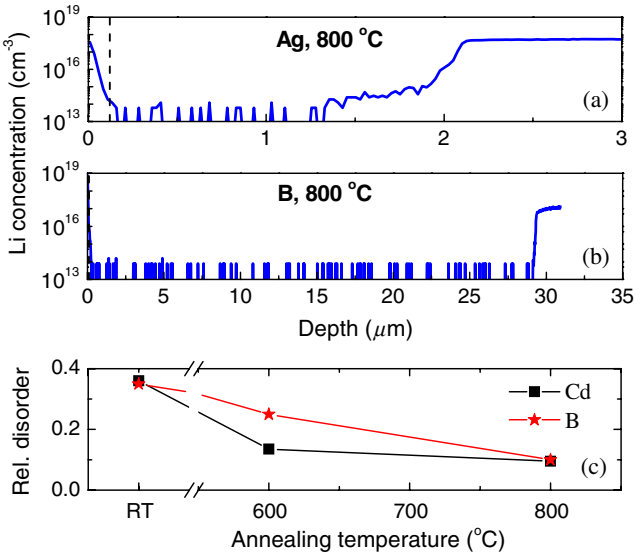

FIG. 2 (color online). Li concentration versus depth profiles in (a) Ag and (b) B implanted ZnO samples after annealing as indicated in the legend (see also Table I for the identification of the samples). The projected ranges of the implanted ions are shown by the vertical dashed lines. (c) Maximum relative disorder [27] in the Zn sublattice for B and Cd implanted samples as a function of annealing temperature.

complexes. Indeed, Fig. 2(c) shows the maximum relative Zn disorder as a function of annealing temperature for the Cd and B implants and the supply of Zn_i surviving 600 °C anneals (assisting Li diffusion at 800 °C) is significantly higher in the latter case, which is attributed to the initially different damage produced by light and heavy ions. Actually, RBS/C results (not shown) indicate that the B implanted samples contain predominantly defect clusters gradually annealing in accordance with Fig. 2(c), while extended defects occur in the Cd implanted ones. These extended defects act as sinks for Zn_i resulting in a II-step annealing, similar to that observed for other heavy implants [19], and therefore, the Li_{Zn} kick-out reaction is partly suppressed.

Extending the argumentation further, we compare the results in Figs. 1 and 2 with that for group-V elements, which, from the electronegativity point of view, are anticipated to occupy O sublattice sites, and Fig. 3 shows corresponding Li versus depth profiles upon annealing at selected temperatures (the rest of the data are omitted for clarity). First, upon N implantation the Li redistribution is qualitatively different compared to that in Figs. 1 and 2 with a pile up at R_p, similar to that observed for O implants and explained in terms of surplus O_i [13], and no depleted region beyond R_p. The Li pileup may be associated with formation of Li_{Zn}-O_i complexes, likely to occur under O-rich conditions [20], and the lack of Li depletion beyond R_p is attributed to incorporation of N (N_2) on O sublattice sites causing no excess of Zn_i but of O_i [21].

Until now the approach of using Li marker diffusion, in form of depleted regions or pileups depending on the actual impurity localization on Zn or O sublattices, has shown consistency with anticipations based on electronegativity. Intriguingly enough, Li redistribution upon P and Sb implants in Fig. 3 resembles that for Zn-substituting elements in Figs 1 and 2, revealing a deep Li depleted region behind R_p, indicating a substantial generation of Zn_i. Concluding that P and Sb directly replace substitutional Zn (forming P_{Zn} and Sb_{Zn}) is unlikely due to inadequate electronic configurations to fit to the surrounding matrix. However, the result in Fig. 3 is consistent with a complex in form of $Sb_{Zn} - 2V_{Zn}$ [1], providing space for accommodation of the excess charge. The same configuration was also suggested for P [22] and, the results in Fig. 3 for P corroborate the formation of corresponding $P_{Zn} - 2V_{Zn}$ complex. Alternatively, the formation of interstitial type complexes with heavy mass group-V impurities in form of X_i-$3V_{Zn}$, as predicted in Ref. [23], are also possible, assuming that Zn_i-s are generated in the course of the V_{Zn} formation. It can be noted that both P and Sb exhibit relatively high values of ΔLi_X compared to other implants used in the present study, with $\Delta Li_P \approx 0.2$ and $\Delta Li_{Sb} \approx 0.1$; this suggests a high generation of Zn_i-s consistent with P(Sb)-multi-V_{Zn} complexes.

Interestingly, Li also accumulates around R_p in the P implanted sample but not in the Sb one (Fig. 3). This may indicate that some fraction of the P atoms reside on O sites giving rise to localized surplus of O_i. Hence, the approach used in the present study has the potential to unveil the prevailing sublattice configuration for amphoteric impurities, i.e., impurities which can occupy substitutional positions in either sublattice, and how the prevalence varies with annealing temperature. Finally, it should be noted that data dealing with Li redistribution in ZnO upon ion implantation and annealing, reported previously in the literature but not fully understood, e.g., Refs. [24–26], are readily explained by the present approach.

In summary, we have found striking correlations between the preferential impurity sublattice occupations and characteristic features of Li diffusion in ZnO, and demonstrated the possibility to use Li as a marker for sublattice localization of a wide variety of implanted elements. In particular, the impurity incorporation into the Zn sublattice (holds for Cd, Mg, B, Ag, Sb, and P) is manifested by remarkable Li-depleted regions extending up to 30 μm beyond R_p, while Li pileup in the region around R_p is induced by impurities residing on O-sites, e.g., N. The phenomena are interpreted in terms of the balance between Zn or O self-interstitials (Zn_i and O_i), so that the residual surplus of Zn_i or O_i determines the actual Li diffusion features. A comparison between Cd(Mg) implants and Cd + O(Mg + O) co-implants reveals that the Zn_i/O_i surplus ratio may be tuned by varying the oxygen implantation parameters.

Financial support from the Norwegian Research Council via FRINAT program is gratefully acknowledged.

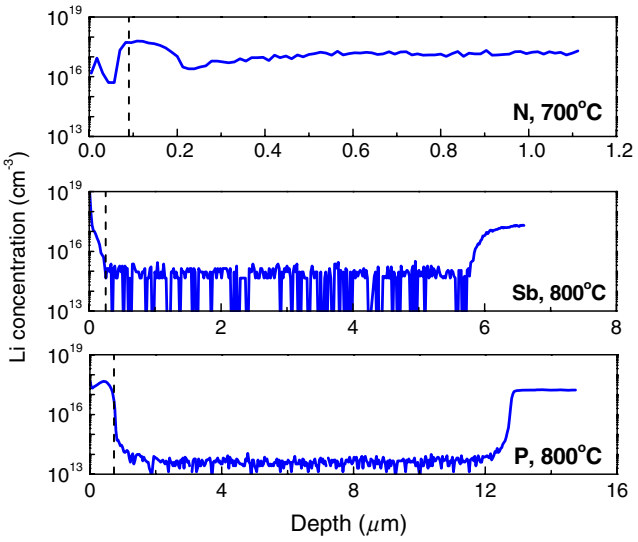

FIG. 3 (color online). Li concentration versus depth profiles in N, Sb, and P implanted ZnO samples after annealing as indicated in the legend (see also Table I for the identification of the samples). The projected ranges of the implanted ions are shown by the vertical dashed lines.

[1] S. Limpijumnong, S. B. Zhang, S.-H. Wei, and C. H. Park, Phys. Rev. Lett. **92**, 155504 (2004).
[2] M. A. Myers, M. T. Myers, M. J. General, J. H. Lee, L. Shao, and H. Wang, Appl. Phys. Lett. **101**, 112101 (2012).
[3] G. Braunstein, A. Muraviev, H. Saxena, N. Dhere, V. Richter, and R. Kalish, Appl. Phys. Lett. **87**, 192103 (2005).
[4] T. M. Barnes, K. Olson, and C. A. Wolden, Appl. Phys. Lett. **86**, 112112 (2005).
[5] F. X. Xiu, Z. Yang, L. J. Mandalapu, D. T. Zhao, J. L. Liua, and W. P. Beyermann, Appl. Phys. Lett. **87**, 152101 (2005).
[6] A. Tsukazaki, H. Saito, K. Tamura, M. Ohtani, H. Koinuma, M. Sumiya, S. Fuke, T. Fukumura, and M. Kawasaki, Appl. Phys. Lett. **81**, 235 (2002).
[7] Y. Cui and F. Bruneval, Appl. Phys. Lett. **97**, 042108 (2010).
[8] L. C. Feldman, J. W. Mayer, and S. T. Picraux, *Materials Analysis by Ion Channeling* (Academic Press, New York, 1982).
[9] G. Amsel and W. A. Lanford, Annu. Rev. Nucl. Part. Sci. **34**, 435 (1984).
[10] H. Hofsäss and G. Lindner, Phys. Rep. **201**, 121 (1991).
[11] P. A. Lee, P. H. Citrin, P. Eisenberger, and B. M. Kincaid, Rev. Mod. Phys. **53**, 769 (1981).
[12] J. E. Stehr, B. K. Meyer, and D. M. Hofmann, Appl. Magn. Reson. **39**, 137 (2010).
[13] P. T. Neuvonen, L. Vines, B. G. Svensson, and A. Yu. Kuznetsov, Phys. Rev. Lett. **110**, 015501 (2013).
[14] J. F. Ziegler, J. P. Biersack, and U. Littmark, *The Stopping and Range of Ionsin Solids* (Pergamon, New York, 1985), Vol. 1, p. 109, www.srim.org.
[15] Another alternative may be to use an atmosphere containing both Zn and O, for example, in an evacuated ampule maintaining conditions closer to the equilibrium. However, in order to avoid any possible risk of impurity cross contaminations potentially coming from the ZnO powder and/or the ampule itself, the anneals were performed in air, which was found to be sufficient in terms of avoiding major modifications of the surface at the temperatures of the experiment; see, e.g., T. M. Børseth, B. G. Svensson, and A. Yu. Kuznetsov, Phys. Scr. **T126**, 10 (2006); C. J. Pan, J. Y. Chen, G. C. Chi, B. W. Chou, B. J. Pong, F. Ren, C. Y. Chang, and S. J. Pearton, Vacuum **83**, 1073 (2009).
[16] A. Carvalho, A. Alkauskas, A. Pasquarello, A. K. Tagantsev, and N. Setter, Phys. Rev. B **80**, 195205 (2009).
[17] P. T. Neuvonen, L. Vines, A. Yu. Kuznetsov, B. G. Svensson, X. L. Du, F. Tuomisto, and A. Hallén, Appl. Phys. Lett. **95**, 242111 (2009).
[18] V. Venkatachalapathy, A. Galeckas, M. Trunk, T. C. Zhang, A. Azarov, and A. Yu. Kuznetsov, Phys. Rev. B **83**, 125315 (2011).
[19] A. Yu. Azarov, A. Hallén, B. G. Svensson, and A. Yu. Kuznetsov, J. Phys. D **45**, 235304 (2012).
[20] M. G. Wardle, J. P. Goss, and P. R. Briddon, Phys. Rev. B **71**, 155205 (2005).
[21] X. H. Li, H. Y. Xu, X. T. Zhang, Y. C. Liu, J. W. Sun, and Y. M. Lu, Appl. Phys. Lett. **95**, 191903 (2009).
[22] W.-J. Lee, J. Kang, and K. J. Chang, Phys. Rev. B **73**, 024117 (2006).
[23] B. Puchala and D. Morgan, Phys. Rev. B **85**, 195207 (2012).
[24] T. M. Børseth, J. S. Christensen, K. Maknys, A. Hallén, B. G. Svensson, and A. Yu. Kuznetsov, Superlattices Microstruct. **38**, 464 (2005).
[25] T. M. Børseth, F. Tuomisto, J. S. Christensen, E. V. Monakhov, B. G. Svensson, and A. Yu. Kuznetsov, Phys. Rev. B **77**, 045204 (2008).
[26] L. Vines, P. T. Neuvonen, A. Yu. Kuznetsov, J. Wong-Leung, C. Jagadish, and B. G. Svensson, Mater. Res. Soc. Symp. Proc. **1394**, 529 (2012).
[27] "Relative disorder" was calculated from RBS/C spectra as an effective number of scattering centers in Zn-sublattice normalized to the atomic concentration (4.15×10^{22} Zn/cm^3).